PCCP

COMMUNICATION

View Article Online
View Journal | View Issue

Published on 12 September 2014. Downloaded by Michigan State University on 28/01/2016 01:33:11.

Cite this: *Phys. Chem. Chem. Phys.*, 2014, **16**, 22953

Received 11th July 2014,
Accepted 12th September 2014

DOI: 10.1039/c4cp03043e

www.rsc.org/pccp

A three-dimensional hierarchical TiO_2 urchin as a photoelectrochemical anode with omnidirectional anti-reflectance properties†

Weina Ren,[a] Haifeng Zhang,[a] Dezhi Kong,[a] Bo Liu,[a] Yaping Yang[a] and Chuanwei Cheng*[ab]

In this communication, we report an innovative electrode design of 3D hierachical TiO_2 urchin assembled with a hollow TiO_2 spheres core and radial TiO_2 nanorod shell prepared *via* a facile colloid template route combined with atomic layer deposition and a hydrothermal growth process. The periodically hierarchical TiO_2 urchin exhibits excellent omnidirectional anti-reflectance properties in a wide range of wavelengths and angles of incidence (AOI). When tested as a photoanode for PEC water splitting, a greatly improved photoelectrochemical water splitting performance is obtained in comparison to that of TiO_2 microspheres due to the improved light harvesting and charge collection efficiency.

Photoelectrochemical water splitting, as a promising clean energy utilization approach *via* harvesting and storing of the solar light in a chemical fuel, H_2 has received increasing research attention.[1–5] In the past few years, great effort has been devoted to develop the photoelectrode materials to boost the solar light to hydrogen conversion efficiency.[6–10] Titanium dioxide (TiO_2), with the advantages of excellent chemical stability, high photoactivity and earth-abundance has been extensively investigated as a photoanode in this area.[11–15] Currently, the rational design of nanoarchitectured photoelectrodes plays an important role in tailoring the photoelectrochemical water splitting performance.[16–22] For example, 1D semiconductor nanowire structures decoupling the light absorption and charge transportation are beneficial for improving the light harvesting and charge collection.[23,24] In general, an ideal photoelectrode architecture should offer a large surface area for interfacial charge collection, long optical path and low light reflectance loss for effective light harvesting and short diffusion distance for excellent charge transportation. In this regard, three dimensional (3D) urchin-like hierarchical structures that combine both 3D and 1D building blocks satisfy all the merits mentioned, which may greatly boost the efficiency.[25–27] Besides, due to the fact that the position of the sun changes through day and year and a large amount of the solar light is incident at all angles-of-incidence (AOIs) as diffused light scattered by the earth's atmosphere, the omnidirectional light harvesting characteristics of the photoelectrode are also very important for high-efficiency photoelectrochemical water splitting devices.[28,29]

Herein, we report the fabrication novel 3D hierarchical urchin-like TiO_2 structures on a transparent conductive FTO glass substrate for the first time by a combination of self-assembled colloidal spheres as a sacrificial template and atomic layer deposition as well as a subsequent low temperature hydrothermal growth. The as-prepared TiO_2 urchin shows excellent light anti-reflectance properties in a wide range of wavelengths and angles of incidence (AOIs) due to its 3D periodically hierarchical structure. As a proof-of-concept application, the photoelectrochemical water splitting function of the TiO_2 urchin is demonstrated, presenting excellent performances with a maximum photocurrent of 0.9 mA cm^{-2}, which is 4.5 times larger than that of the control electrode of TiO_2 microsphere arrays.

The fabrication processes for urchin-like TiO_2 structures consist of five steps as schematically illustrated in Fig. 1.

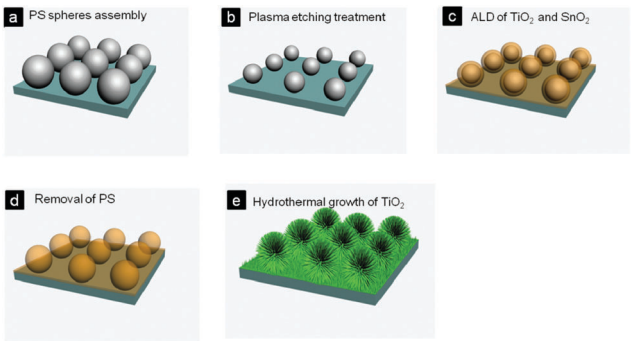

Fig. 1 Scheme of the fabrication processes of the urchin-like TiO_2.

[a] *MOE Key Laboratory of Advanced Micro-structured Materials, School of Physics Science and Engineering, Tongji University, Shanghai 200092, P. R. China. E-mail: cwcheng@tongji.edu.cn*

[b] *National Laboratory for Infrared Physics, Shanghai Institute of Technical Physics, Chinese Academy of Sciences, Shanghai 200083, P. R. China*

† Electronic supplementary information (ESI) available: Long-term stability test results and equivalent circuit and parameters. See DOI: 10.1039/c4cp03043e

Published on 12 September 2014. Downloaded by Michigan State University on 28/01/2016 01:33:11.

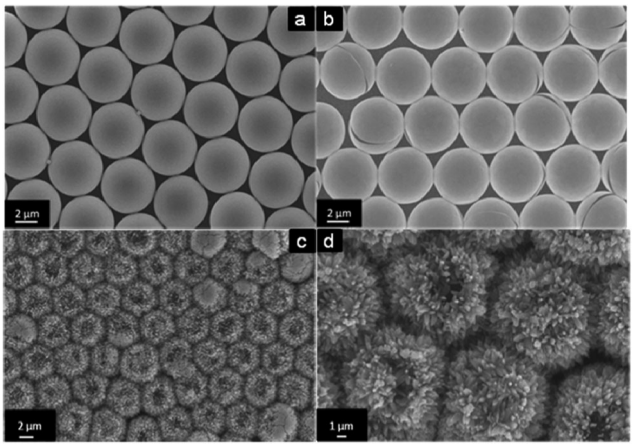

Fig. 2 SEM image of (a) monolayer PS microsphere arrays assembled on the FTO substrate; (b) TiO_2 hollow microsphere arrays; (c) and (d) urchin-like TiO_2 arrays.

First, a monolayer of PS microspheres was assembled onto the FTO glass substrate. Then the sizes of the PS spheres were reduced by an oxygen plasma etching process. After that, 35 nm of TiO_2 and 10 nm of SnO_2 layers were deposited onto the microsphere surface by ALD. Subsequently, the PS microspheres were burned off by calcination, leaving spherical voids in the TiO_2 structures. Finally, TiO_2 nanorods were grown on the surfaces of each hollow TiO_2 sphere by a hydrothermal process. It is worth noting that the SnO_2 layer is critical to facilitate the TiO_2 nanorods growth due to the small lattice mismatches between SnO_2 and rutile TiO_2.

As shown in Fig. 2a, a well-organized monolayer of polystyrene (PS) microspheres can be observed in a large area. After the ALD of TiO_2 and removal of PS spheres, the microspheres still retain the well ordered structure with smooth surfaces and hollow voids, as demonstrated in Fig. 2b. Fig. 2c and d depict the SEM images of the as-prepared urchin-like TiO_2 structures. It can be observed that groups of freestanding TiO_2 nanorods are branching out from the surfaces of each hollow TiO_2 microsphere, exhibiting a "sea-urchin"-like shape. The diameters and the length of the TiO_2 nanorods are $\sim$30 nm and 100–200 nm, respectively. As seen in Fig. 2d, the diameter of the hollow void is about 4 μm. The growth mechanism of TiO_2 urchin can be proposed as follows. First, the Ti^4 precursors hydrolyze with water, resulting in the formation of crystal nucleus on the hollow TiO_2/SnO_2 surface. Then with continuous hydrolysis and subsequent growth-crystallization, TiO_2 nanorods are radially branched out, forming a "sea urchin" shape, due to the favored anisotropic growth of rutile TiO_2.[12]

The structural information of the TiO_2 urchin is further analyzed using HRTEM and selected area electron diffraction (SAED). As shown in Fig. 3a, the TiO_2 nanorods are assembled by nanoparticles with a bundle structure. The HRTEM image and SAED in Fig. 3b confirm the TiO_2 nanorods possess a single-crystalline rutile structure. The measured lattice spacing is $\sim$2.4 Å, which is consistent with the *d*-spacing of the tetragonal (101) planes of TiO_2.

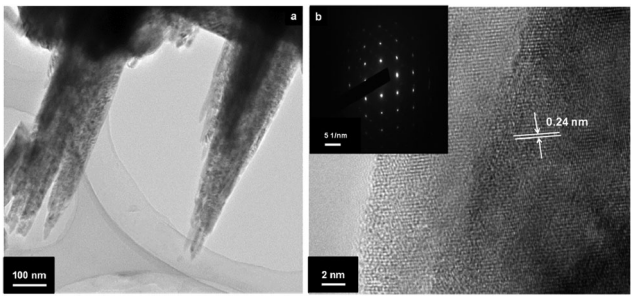

Fig. 3 (a) TEM image and (b) HRTEM image of TiO_2 nanorods, inset in Fig. 2b is the SAED patterns.

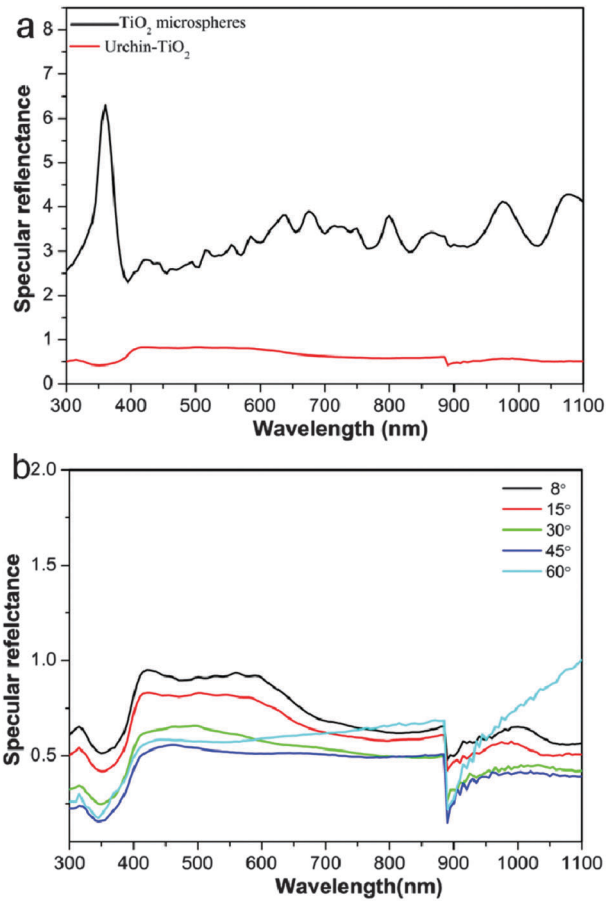

Fig. 4 (a) Specular reflectance spectra of TiO_2 microspheres and TiO_2 urchin at an incident angle of 8° (b) specular reflectance spectra of TiO_2 urchin arrays at different angles of incidence.

To determine the anti-reflectance properties of the TiO_2 microspheres and TiO_2 urchin-like structures, specular reflectance spectra in the broad wavelength range of 300–1100 nm were measured. Fig. 4a compares the specular reflectance spectra of the TiO_2 microspheres and TiO_2 urchin-like structures measured at an incident angle of 8°. It can be seen that the urchin-like TiO_2 structures present much lower light reflectance in the whole measured wavelength. The excellent anti-reflectance properties for TiO_2 urchin might be due to the strong light scattering effect caused by the periodically

 This journal is © the Owner Societies 2014

Published on 12 September 2014. Downloaded by Michigan State University on 28/01/2016 01:33:11.

hierarchical structures that enhance the light–matter interaction.[30] To further reveal their omnidirectional anti-reflection properties, the specular reflectance spectra of the urchin-like TiO_2 arrays at different incident angles were measured. As shown in Fig. 4b, it is clear that the urchin-like TiO_2 arrays exhibit a prominent anti-reflection behaviour toward wide angles of incidence from 8° to 60° with reflection <1% in the broad wavelength range of 300–1100 nm, indicating excellent omnidirectional anti-reflection properties. The broad and omnidirectional anti-reflection abilities of the urchin-like TiO_2 are beneficial for the incoming light to undergo multiple scattering and thereby reduce the overall surface reflectance.

As a proof-of-concept application, the as fabricated 3D urchin-like TiO_2 structures were investigated as a photoanode for photoelectrochemical water splitting. The photoelectrochemical water splitting measurements were conducted in a three-electrode configuration with the urchin TiO_2 as the working electrode, a Pt foil as the counter electrode and an Ag/AgCl electrode as the reference electrode. For comparison, the performance of the hollow TiO_2 microsphere electrode was measured as a reference. Fig. 5a shows the linear sweep voltammetry curves of the two sets of samples measured in the dark and under simulated light illumination. One can see that both the samples have negligible photocurrent in the dark, while under light illumination, an obvious photocurrent is generated from the TiO_2 microspheres and urchin-like TiO_2 electrodes, indicating that efficient charge generation and separation have occurred at the semiconductor/electrolyte interface. By a careful observation of the photocurrent *vs.* potential curve of the urchin-like TiO_2 electrode, the photocurrent density gradually increases since the onset potential of −0.8 V *vs.* Ag/AgCl, and approaches a saturation value of ~0.9 mA cm^{-2} at −0.5 *vs.* Ag/AgCl, which is about 4.5 times larger than that of TiO_2 microsphere photoanode. The measured photocurrent density from the urchin-like TiO_2 electrode is also much superior to that of conventional P25 nanoparticle films photoanode reported by others.[21]

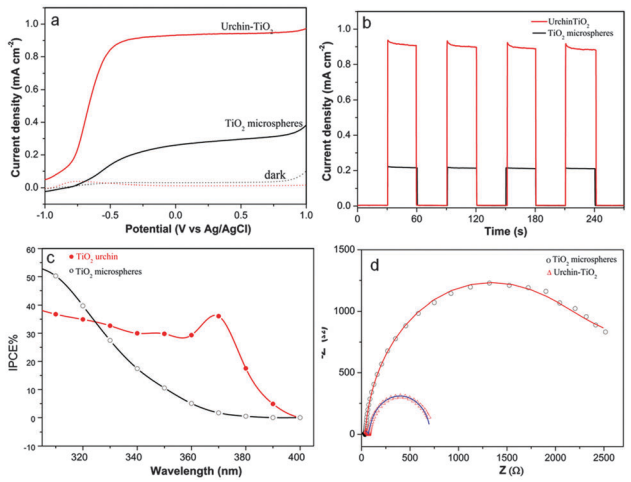

Fig. 5 (a) Linear sweep voltammetry measurements of the urchin-like TiO_2 and TiO_2 microspheres electrodes, collected both in the dark and 100 mW cm^{-2} simulated sunlight illumination. (b) Amperometric *I*–*t* curves at an applied bias of 0 V at 100 mW cm^{-2} illumination with 30 s light on–off cycles. (c) IPCE spectra of the urchin-like TiO_2 and TiO_2 microsphere electrode collected at 0 V *vs.* Ag/AgCl. (d) Measurement of the electrochemical impedance spectra in Nyquist plots.

Fig. 5b shows the corresponding transient photocurrent *vs.* time curves of the urchin-like TiO_2 and TiO_2 microsphere electrodes measured under light illumination with 30 s light On–Off cycles. It can be seen that the urchin-like TiO_2 shows a good photo-switching performance with fast response and recovery times. Good long-term stability is also demonstrated for the urchin-like TiO_2 electrode with the continuous light illumination test (see Fig. S1, ESI†).

The improved PEC performance for the 3D urchin-like TiO_2 electrode might be attributed to the following reasons. First, the 3D hierarchical structures provided increased surface area and strong light trapping effect, resulting in enhanced light harvesting. Second, the hydrothermal-grown single-crystalline nature of rutile TiO_2 urchin is able to reduce the charge recombination loss greatly in contrast to ALD anatase TiO_2.[22,31] Third, the urchin structures that consisted of hollow spheres combined with 1D TiO_2 nanorods offered increased photoanode/electrolyte contact areas, which facilitated the charge separation and transfer process, leading to improvement of the charge collection efficiency.

To quantitatively investigate the wavelength-dependent photoactivity of the urchin-like TiO_2 electrode, IPCE measurements were conducted with a three-electrode configuration at 0 V *vs.* Ag/AgCl. The IPCE values were calculated from the following equation:

$$\mathrm{IPCE} = (1240I)/(\lambda J_{\mathrm{light}}) \quad (1)$$

where I is the measured photocurrent density, λ is the wavelength of the incident light and J_{light} is the measured irradiance at the specific wavelength. As shown in Fig. 5c, the urchin like-TiO_2 presents excellent photoresponse over the entire measured wavelength of 300–400 nm in contrast to that of a TiO_2 microsphere electrode, and a maximum IPCE value of 35% at the wavelength of 370 nm is observed, which is consistent with the bandgap absorption characteristic of rutile TiO_2.

To investigate the charge and transfer process of urchin like-TiO_2 photoelectrode, electrochemical impedance spectroscopy (EIS) measurements were conducted under open-circuit conditions under simulated solar light illumination. Fig. 5d shows the Nyquist plots of the obtained EIS data. The high frequency ($>10^4$ Hz) semicircle portion in the Nyquist plots corresponds to the charge transfer in the TiO_2/FTO interface, and the second semicircle in the middle frequency range (1–10^3 Hz) represents the charge transfer at the TiO_2/electrolyte interface. The measured impedance spectroscopic data were fitted by using an equivalent circuit (Fig. S2, ESI†) and Zsimpwin software.[32] The fitted parameters are summarized in Table S1 in ESI.† The urchin-TiO_2 electrode shows decreased charge transfer resistance in comparison to that of the TiO_2 microspheres one, indicating that the urchin-like structures are facilitating the charge separation and transportation arising from the increased contact surface area.

Published on 12 September 2014. Downloaded by Michigan State University on 28/01/2016 01:33:11.

Conclusions

In conclusion, we have fabricated novel 3D urchin-like TiO_2 hierarchical structures by combination of a colloidal template and solution synthesis, which exhibits favorable omnidirectional broadband light anti-reflectance properties. The excellent photon management of urchin-like TiO_2 allows for its use as a photoanode in PEC water splitting applications, achieving a maximum photocurrent density of $\sim$0.9 mA cm^{-2}, which is 4.5 times larger than that of TiO_2 microsphere arrays. This simple fabrication method might be adopted to fabricate a wide variety of other 3D periodically hierarchical structures that find applications in optoelectronic devices, sensing and so on.

Experimental section

Preparation of urchin-like TiO_2

Fluorine-doped SnO_2 (FTO) coated glass substrates (15 Ω^{-1}) were cleaned by immersed in acetone and ethanol for 10 min each with sonication and dried under an N_2 stream. After that, monolayer commercial monodispersed carboxylate-modified polystyrene (PS) spheres with diameters of 4.5 μm (*Alfa Aesar*, 2.5 wt% aqueous dispersion) were assembled onto the FTO coated glass substrates. Subsequently, the sizes of the self-assembled monolayer PS microspheres were reduced by an O_2 plasma etching process.

After that, the PS microspheres were coated with 35 nm TiO_2 and 10 nm SnO_2 by an atomic layer deposition system (Picsun SUNALE R-200), respectively. Titanium tetrachloride, tin(IV) chloride, and H_2O were used as the Ti, Sn and O precursors, respectively. During the deposition, the reaction chamber was maintained at 1.0 mbar with a steady N_2 gas at 200 sccm (cubic centimeter per minute). Each ALD cycle consisted of a 500 ms precursor pulse and 3 s purging time with N_2. The film thickness was controlled by the numbers of the ALD cycles. TiO_2 was deposited at 75 °C to avoid melting of the PS sphere, and 850 cycles were used to deposit about 35 nm thick TiO_2. Subsequently, the original PS spheres were removed by calcination in air at 450 °C for 1 h, leaving spherical voids in the TiO_2 structure. To facilitate the growth of TiO_2, SnO_2 was deposited at 400 °C by 80 cycles with 10 nm thickness. Finally, TiO_2 nanorods were grown on the surface of the hollow TiO_2/SnO_2 infiltrated opals using a hydrothermal method.[22] The ALD TiO_2 and SnO_2 coated substrate was immersed into a 50 ml sealed Teflon-lined stainless steel autoclave containing 15 ml of toluene, 0.45 ml of tetrabutyl titanate and 0.5 ml of hydrochloric acid. The hydrothermal process was conducted at 150 °C for 3 h. After the reactions, the substrates were removed from the solution, rinsed with deionized water, and dried with N_2.

Characterizations

The morphology and microstructures of the as prepared urchin TiO_2 samples were characterized using FEI Sirion200 emission scanning electron microscopy (FE-SEM), and a JEM 2010F transmission electron microscope (TEM). The specular reflectance spectra were recorded on a UV/Vis/NIR spectrophotometer (PerkinElmer Lambda 950).

Photoelectrochemical measurements

The PEC performance of the electrodes was measured in a three-electrode configuration under simulated AM1.5G illumination using a potentiostat (CHI760D, CH instrument). The as-prepared samples were used as working electrodes, and the Ag/AgCl in saturated KCl (+0.197 V *vs.* NHE), and a Pt foil were used as the reference electrode and the counter electrode, respectively. The electrolyte was 1 M NaOH solution with PH of $\sim$14. The photoresponse was measured under chopped irradiation from a 150 W Xe lamp (Zolix SS150) equipped with an AM1.5 G filter, calibrated using a standard Si solar cell to simulate AM1.5 illumination (100 mW cm^{-2}). Time-dependent photoresponse tests were carried out by measuring the photocurrent under chopped light irradiation (light–dark cycles of 30 s) at a fixed bias of 0 V *vs.* Ag/AgCl. The incident-photon-to-electron conversion efficiency (IPCE) was collected as a function of wavelength from 300 to 600 nm using a specially designed IPCE system (Zolix Solar cell Scan100) with three electrodes configuration under 0 V *vs.* Ag/AgCl. Electrochemical impedance spectra were measured on a potentiostat (CHI760 D, CH instrument) by applying a bias of the open-circuit voltage over a frequency range of 10^{-1} to 10^5 Hz with a 5 mV amplitude under 100 mW cm^{-2} illumination.

Acknowledgements

This work was financially supported by the 973 Program (Grant no. 2013CB632701), the National Natural Science Foundation of China (Grant no. 51202163), the Shanghai Pujiang Program (Grant no. 12PJ1408200), the Innovation Program of Shanghai Municipal Education Commission (Grant no. 13ZZ025), Doctor Programs Foundation of MOE (20120072120044), the Open Fund Project of National Laboratory for Infrared Physics (Grant No. M201302) and the Fundamental Research Fund for Central University.

Notes and references

1 J. W. Sun, D. K. Zhong and D. R. Gamelin, *Energy Environ. Sci.*, 2010, **3**, 1252.
2 M. G. Walter, E. L. Warren, J. R. McKone, S. W. Boettcher, Q. X. Mi, E. A. Santori and N. S. Lewis, *Chem. Rev.*, 2010, **110**, 6446.
3 X. B. Chen and S. S. Mao, *Chem. Rev.*, 2007, **107**, 2891.
4 Y. Li and J. Z. Zhang, *Laser Photonics Rev.*, 2009, **4**, 517.
5 Y. Tachibana, L. Vayssieres and J. R. Durrant, *Nat. Photonics*, 2012, **6**, 511.
6 S. W. Boettcher, J. M. Spurgeon, M. C. Putnam, E. L. Warren, D. B. Turner-Evans, M. D. Kelzenberg, J. R. Maiolo, H. A. Atwater and N. S. Lewis, *Science*, 2010, **327**, 185.
7 C. X. Kronawitter, L. Vayssieres, S. H. Shen, L. J. Guo, D. A. Wheeler, J. Z. Zhang, B. R. Antoun and S. S. Mao, *Energy Environ. Sci.*, 2011, **4**, 3889.

 This journal is © the Owner Societies 2014

Published on 12 September 2014. Downloaded by Michigan State University on 28/01/2016 01:33:11.

8 A. Paracchino, V. Laporte, K. Sivula, M. Grätzel and E. Thims, *Nat. Mater.*, 2011, **10**, 456.
9 J. H. Park, S. W. Kim and A. J. Bard, *Nano Lett.*, 2006, **6**, 24.
10 E. Garnett and P. D. Yang, *Nano Lett.*, 2010, **10**, 1082.
11 A. Wolcott, W. A. Smith, T. R. Kuykendall, Y. P. Zhao and J. Z. Zhang, *Small*, 2009, **5**, 104.
12 X. Feng, K. Shankar, O. K. Varghese, M. Paulose, T. J. Latempa and C. A. Grimes, *Nano Lett.*, 2008, **8**, 3871.
13 P. Hartmann, D. K. Lee, B. M. Smarsly and J. Janek, *ACS Nano*, 2010, **4**, 3147.
14 C. W. Cheng and Y. Sun, *Appl. Surf. Sci.*, 2012, **263**, 273.
15 G. M. Wang, H. Y. Wang, Y. C. Ling, Y. C. Tang, X. Y. Yang, R. C. Fitzmorris, C. C. Wang, J. Z. Zhang and Y. Li, *Nano Lett.*, 2011, **11**, 3026–3033.
16 C. W. Cheng, Y. Y. Tay, H. H. Hng and H. J. Fan, *J. Mater. Res.*, 2011, **26**, 2254.
17 J. Shi, Y. Hara, C. L. Sun, M. A. Anderson and X. D. Wang, *Nano Lett.*, 2011, **11**, 3412.
18 Y. J. Lin, S. Zhou, S. W. Sheehan and D. W. Wang, *J. Am. Chem. Soc.*, 2011, **133**, 2398.
19 C. W. Cheng, S. K. Karuturi, L. J. Liu, J. P. Liu, H. X. Li, L. T. Su, A. I. Y. Tok and H. J. Fan, *Small*, 2012, **8**, 37.
20 S. K. Karuturi, C. W. Cheng, L. Liu, L. T. Su, H. J. Fan and A. I. Y. Tok, *Nano Energy*, 2012, **1**, 322.
21 I. S. Cho, Z. Chen, A. J. Forman, D. R. Kim, P. M. Rao, T. F. Jaramillo and X. L. Zheng, *Nano Lett.*, 2011, **11**, 4978.
22 C. W. Cheng, W. N. Ren and H. F. Zhang, *Nano Energy*, 2014, **5**, 132.
23 L. S. Li, Y. H. Yu, F. Meng, Y. Z. Tan, R. J. Hamers and S. Jin, *Nano Lett.*, 2012, **12**, 724.
24 C. Liu, N. Dagupta and P. D. Yang, *Chem. Mater.*, 2014, **1**, 26.
25 J. Elias, C. Lévy-clément, M. Bechelany, J. Michler, G.-Y. Wang, Z. Wang and L. Philippe, *Adv. Mater.*, 2010, **22**, 1067.
26 D.-M. Tang, G. Liu, F. Li, J. Tan, C. Liu, G. Q. Lu and H. M. Cheng, *J. Phys. Chem. C*, 2009, **113**, 11035.
27 C. W. Cheng, H. F. Zhang, W. N. Ren, W. J. Dong and Y. Sun, *Nano Energy*, 2013, **2**, 799.
28 X. Yan, D. J. Poxson, J. Cho, R. E. Welser, A. K. Sood, J. K. Kim and E. F. Schubert, *Adv. Funct. Mater.*, 2013, **23**, 583.
29 M.-Y. Hsieh, S.-Y. Kuo, H.-V. Han, J.-F. Yang, Y.-K. Liao, F.-I. Lai and H.-C. Kuo, *Nanoscale*, 2013, **5**, 3841.
30 A. Dev, B. D. Choudhury, A. Abedin and S. Anand, *Adv. Funct. Mater.*, 2014, **24**, 4577.
31 Q. Peng, B. Kalanyan, P. G. Hoertz, A. Miller, D. H. Kim, K. Hanson, L. Alibabaei, J. Liu, T. J. Mey, G. N. Parsons and J. T. Glass, *Nano Lett.*, 2013, **13**, 1481.
32 Y. B. Xie, L. M. Zhou and J. Lu, *J. Mater. Sci.*, 2009, **44**, 2907.